CHAPTER 6

MULTIMODE TIME DEPENDENT NONLINEAR ANALYSIS OF GYRO-TWT AMPLIFIER

6.1. Introduction

As discussed earlier, in order to reduce requirement of high DC magnetic field for the high frequency gyro-TWTs, the device is often operated at the harmonic modes. In case of higher harmonic operation, the RF interaction structure cylindrical waveguide has to be operated at the high order modes. For such overmoded waveguides, the mode spectrum becomes very dense and electron beam is probable to interact with the several nearby modes simultaneously, if it is used as the RF interaction structure of the gyro-devices. In case the competing modes amplify and propagate with same phase and group velocities, leads to device instability, increase in losses and lowers the efficiency. The efficiency depends upon the tightness of the electron bunches, difference in the bunching pattern due to different mode in the device leads to the existence of two or more modes simultaneously.

The single mode gyro-TWT device operation is only possible if the design of interaction region is appropriate, the start oscillation current and interaction length criteria are properly selected after due analysis for the designed waveguide. In addition for synchronization, a fundamental-harmonic gyro-TWT requires high DC magnetic field, because the output signal frequency is directly proportional to the magnetic field, $\omega \cong \Omega_c = 1.76 \times 10^{11} B_0(T)/\gamma$ [Wang *et al.* (2000)]. A millimetre wave gyro-TWT generally requires a superconducting magnetic to provide such high static magnetic field. To overcome the high magnetic field requirement, amplifier is to operate at a harmonic of the cyclotron frequency. Higher harmonic modes are difficult to excite due to the mode competition from the fundamental harmonic modes and other nearby competing modes. Hence, the study of multimode interaction mechanism is essential for the harmonic device operating in the millimetre and sub-millimetre wave region.

The nonlinear analysis is used to predict output power, efficiency, and bunching phenomena of electrons thereby providing better understanding of the saturation mechanism. Nonlinear analysis can include the drift of electron guiding center, the effect of velocity spread, and inhomogeneity of applied magnetic field. The arbitrary type of interaction structure can also be comprised in the nonlinear analysis. Another advantage of this method is that the electron overtaking and the saturation effects caused by defocusing of the electron bunch from the RF phase can be taken into account which results in better explanation for the nonlinearity.

The purpose of the present chapter is to study the performance of the overmoded waveguide in the presence of several modes, a nonlinear time dependent multimode analysis is developed. The self-consistent equations to provide information about all the competiting modes simultaneously in the gyro-TWTs are derived. To identify important design parameters for the design of gyro-TWT amplifier a suitable approach for its design is developed. Therefore, in the present work, author is also taken the optimized ceramic wedge loaded *W*-band amplifier as described in previous chapter for the study using the time dependent multimode nonlinear analysis developed in the present chapter.

6.2. Multimode Time-Dependent Analysis

As shown in Figure 1, points O, A are the centre of circular waveguide and beamlet respectively and point B depicts the instantaneous position of electron in the presence of a uniform magnetic field [Wang *et al.* (2014)]. The radius of waveguide, guiding radius, Larmor radius and instantaneous distance of electron from the waveguide centre is r_w, r_b, r_L and r, respectively. In the absence of RF input, beamlets centre is stationary. θ, ψ, ϕ

and $(\pi/2)+\phi-\psi$ are the electron position, guiding centre, polar angle of p_t and gyration phase angle of the cyclotron motion of electrons angle, respectively.

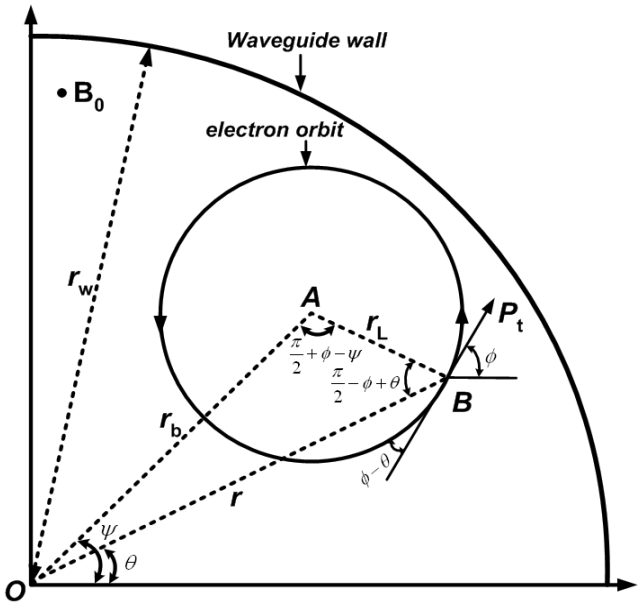

Figure 6.1. Projection of an electron orbit in tranverse plane, showing various orbital parameters.

It is considered that electron beam interacts with the one or more competing modes closely spaced in the waveguide [Wang *et al.* (2013), Wang *et al.* (2014)].

The electric and magnetic fields of TE_{mn} mode in a waveguide can be decomposed as

$$\vec{E} = \vec{E}_t = \vec{E}_r\hat{r} + E_\theta\hat{\theta} \tag{6.1}$$

$$\vec{B} = \vec{B}_t + B_z\hat{e}_z = B_r\hat{r} + B_\theta\hat{\theta} + (B_z + B_0)\hat{z} \tag{6.2}$$

Where, $\vec{E}_t$, $\vec{B}_t$, B_z are the transverse electric, transverse magnetic and axial magnetic field components respectively [Peng *et al.* (2014)]. The right circularly polarized TE_{mn} mode can be expressed in the superposition form of cylindrical coordinate system (r,θ,z) as

$$\vec{E}_t = \mathrm{Re}\sum_{l=1}^{L}\left\{\frac{i\omega\mu_0}{k_{t_l}^2}\,p_l(z,t)\vec{b}_l(r,\theta)\,\mathrm{e}^{\mathrm{i}\omega\mathrm{t}}\right\} \tag{6.3}$$

$$\vec{B}_t = \mathrm{Re}\sum_{l=1}^{L}\left\{\frac{\mu_0}{k_{k_l}^2}\frac{\partial q_l(z,t)}{\partial z}\vec{e}_l(r,\theta)\,\mathrm{e}^{\mathrm{i}\omega t}\right\} \tag{6.4}$$

$$B_z = \mathrm{Re}\sum_{l=1}^{L}\left\{\mu_0 q_l(z,t)\Psi_l(r,\theta)\,\mathrm{e}^{i\omega t}\right\} \tag{6.5}$$

Where, L is the number of interacting modes, $k_{mn} = v_{mn}/r_w$, v_{mn} is the n^{th} root of $J'(x) = 0$, SI unit system is adopted and transverse profile is expressed as

$$\Psi_l\left(\mathrm{r},\theta\right) = J_{m_l}(k_{t_l} r)\,\mathrm{e}^{-im_l\theta} \tag{6.6}$$

$$\vec{e}_l(r,\theta) = \nabla_t \Psi_l \tag{6.7}$$

$$\vec{b}_l(r,\theta) = \hat{z}\times\vec{e}_l \tag{6.8}$$

where functions $\vec{e}_l(r,\theta)$, $\vec{b}_l(r,\theta)$ and $\Psi_l(\mathrm{r},\theta)$ describe the transverse field profiles in the waveguide, and $p_l(z,t)$, $q_l(z,t)$ is the complex amplitude of the corresponding mode, which depend upon mode, axial position and time [Wang *et al.* (2014)]. The scalar function satisfies the Helmholtz equation with respect to transverse coordinates.

$$\left(\nabla_t + k_{t_l}^2\right)\Psi_l = 0 \tag{6.9}$$

and the boundary condition on the waveguide

$$\frac{\partial \Psi_l}{\partial n} = 0 \tag{6.10}$$

where $\partial/\partial n$ denotes the normal derivative. The vector function satisfy the following orthonormality condition when integrated over the waveguide cross-section

$$\int_a da\mathrm{h}_{ni}.\mathrm{h}_{nj} = \delta_{ij} \tag{6.11}$$

where $\vec{h}$ denotes either $\vec{e}(r,\theta)$ or $\vec{b}(r,\theta)$ and the Kronecker delta function

$$\delta_{ij} = 1 \quad \text{if} \quad i = j, \quad \delta_{ij} = 0 \quad \text{if} \quad i \neq j \tag{6.12}$$

The Maxwell's equation

$$\nabla \times \vec{E} = -\frac{\partial \vec{B}}{\partial t} \tag{6.13}$$

$$\nabla \times \vec{B} = \mu_0 \vec{J} + \frac{1}{c^2}\frac{\partial \vec{E}}{\partial t} \tag{6.14}$$

to obtain

$$\nabla^2 \vec{E} = \frac{1}{c^2}\frac{\partial^2 \vec{E}}{\partial t^2} + \mu_0 \frac{\partial J}{\partial t} \tag{6.15}$$

by substituting the RF field expression from equation (6.3)-(6.5) into equation (6.15), after some simplification we can obtain

$$p_l = q_l + \frac{1}{i\omega}\frac{\partial q_l}{\partial t} \tag{6.16}$$

$$\frac{1}{c^2}\frac{\partial^2 q_l}{\partial t^2} + \frac{2ik}{c}\frac{\partial q_l}{\partial t} - \frac{\partial^2 q_l}{\partial z^2} - k_z^2 q_l + S_l = 0 \tag{6.17}$$

equation (6.17) are the partial differential equation of p, q and S.

$$S_l = \frac{\omega}{\pi C_l^2}\int_0^{2\pi/\omega}\int \vec{J}_t.\vec{e}_l^{\,*}\; e^{-i\omega t}\,da\,dt \tag{6.18}$$

where $C_l^2 = \pi r_w^2\left(1 - m_l^2/v_{t_l}^2\right)J_{m_l}^2(v_{t_l})$ is the normalized constant and $\vec{J}_t$ is transverse density of the electron beam. The term $\vec{J}_t.\vec{e}_l^{\,*}$ describes the energy transfer between wave and beam of l^{th} mode. We use the Graff's summation theorem for Bessel function to express the transverse field profile as a sum of infinite number of harmonics in guiding centre coordinates (ρ, φ, z),

$$\Psi_l(r,\theta) = \sum_{s=-\infty}^{s=\infty} J_s(k_{t_l} r_L) J_{m-s}(k_{t_l} r_b)\, e^{-i(m_l - s)\psi - is\varphi} \tag{6.19}$$

$$e_l(r,\theta)=\sum_{s=-\infty}^{s=\infty}\left(k_{t_l}J_s'(k_{t_l}r_L)\hat{\rho}-\frac{is}{\rho_L}J_s(k_{t_l}r_L)\hat{\varphi}\right)J_{m-s}(k_{t_l}r_b)\,\mathrm{e}^{-i(m_l-s)\psi-\mathrm{i}s\varphi} \tag{6.20}$$

$$b_l(r,\theta)=\sum_{s=-\infty}^{s=\infty}\left(\frac{is}{r_L}J_s(k_{t_l}r_L)\hat{\rho}+k_{t_l}J_s'(k_{t_l}r_L)\hat{\varphi}\right)J_{m-s}(k_{t_l}r_b)\,\mathrm{e}^{-i(m_l-s)\psi-\mathrm{i}s\varphi} \tag{6.21}$$

Put the value from equation (6.19)-(6.21) into equation (6.3)-(6.5), obtain the electric and magnetic of corresponding mode field component in terms of Bessel function

$$\vec{E}_\rho=\mathrm{Re}\sum_{l=1}^{L}\left\{\sum_{s=-\infty}^{s=\infty}-\frac{\mu_0 s\omega}{r_L k_{t_l}^2}p_l(z,t)J_s(k_{t_l}r_L)J_{m-s}(k_{t_l}r_b)\,\mathrm{e}^{i(\omega t-(m_l-s)\psi-\mathrm{i}s\varphi)}\right\} \tag{6.22}$$

$$\vec{E}_\varphi=\mathrm{Re}\sum_{l=1}^{L}\left\{\sum_{s=-\infty}^{\infty}i\frac{\mu_0\omega}{k_{t_l}}p_l(z,t)J_s'(k_{t_l}r_L)J_{m-s}(k_{t_l}r_b)\,\mathrm{e}^{i(\omega t-(m_l-s)\psi-\mathrm{i}s\varphi)}\right\} \tag{6.23}$$

$$\vec{E}_z=0 \tag{6.24}$$

$$\vec{B}_\rho=\mathrm{Re}\sum_{l=1}^{L}\left\{\sum_{s=-\infty}^{\infty}\frac{\mu_0}{k_{t_l}}\frac{\partial q_l(z,t)}{\partial z}J_s'(k_{t_l}r_L)J_{m-s}(k_{t_l}r_b)\,\mathrm{e}^{i(\omega t-(m_l-s)\psi-\mathrm{i}s\varphi)}\right\} \tag{6.25}$$

$$\vec{B}_\theta=\mathrm{Re}\sum_{l=1}^{L}\left\{\sum_{s=-\infty}^{\infty}-i\frac{\mu_0 s}{k_{t_l}^2 r_L}\frac{\partial q_l(z,t)}{\partial z}J_s(k_{t_l}r_L)J_{m-s}(k_{t_l}r_b)\,\mathrm{e}^{i(\omega t-(m_l-s)\psi-\mathrm{i}s\varphi)}\right\} \tag{6.26}$$

$$B_z=\mathrm{Re}\sum_{l=1}^{L}\left\{\sum_{s=-\infty}^{s=\infty}\mu_0 q_l(z,t)J_s(k_{t_l}r_L)J_{m-s}(k_{t_l}r_b)\,\mathrm{e}^{i(\omega t-(m_l-s)\psi-\mathrm{i}s\varphi)}\right\} \tag{6.27}$$

For the electron beam represented by N discrete electrons and v_z is positive for all electron, the current density can be represented as [Chu *et al.* (1999)]

$$\vec{J}_z(\vec{x},t)=\frac{R}{r}\sum_{i=1}^{N}W_i\delta(r-r_i)\delta(\theta-\theta_i)\delta(t-t_i)\vec{v}_i \tag{6.28}$$

where W_i is a normalized weighting factor for the i^{th} electron satisfying

$$\sum_{i=1}^{N}W_i=1 \tag{6.29}$$

and C is determined from the beam current I_b through

$$I_b = \int_0^{r_w} r dr \int_0^{2\pi} d\theta \left\langle J_z \right\rangle_t \tag{6.30}$$

$$\vec{J}_t = \frac{2\pi I_b}{\omega r} \sum_{i=1}^{N} W_i \delta(r - r_i)\delta(\theta - \theta_i)\delta(t - t_i)\frac{\vec{v}_{ti}}{v_{zi}} \tag{6.31}$$

Substituting equation (6.21) and (6.31) into equation (6.18), we get

$$S_l = \frac{2I_b k_{t_l}}{C_l^2}\left(\sum_{i=1}^{N} W_i \frac{\vec{v}_{ti} J_s'(k_{t_l} r_{Li}) J_{m-s}(k_{t_l} r_{bi})}{v_{zi}}\right) e^{-i\omega t_i + (m_l - s)\psi_i + i s\varphi_i} \tag{6.32}$$

For obtaining field amplitude solve partial differential equation. Equation (6.17) can be simplified for convenience, first neglect the second order term $\partial^2 q/\partial t^2$, because its coefficient is much smaller than first order term $\partial q/\partial t$ coefficient, that is $\left|1/c^2\right| \ll \left|2ik/c\right|$.

$$\frac{\partial^2 q_l}{\partial z^2} - \frac{2ik}{c}\frac{\partial q_l}{\partial t} + k_z^2 q_l = S_l \tag{6.33}$$

Put the value of S_l

$$\frac{\partial^2 q_l}{\partial z^2} - \frac{2ik}{c}\frac{\partial q_l}{\partial t} + k_{z_l}^2 q_l = \frac{2I_b k_{t_l}}{C_l^2}\left(\sum_{i=1}^{N} W_i \frac{\vec{v}_{ti} J_s'(k_{t_l} r_{L_i}) J_{m-s}(k_{t_l} r_{b_i})}{v_{zi}}\right) e^{-i\omega t_i + (m_l - s)\psi_i + i s\varphi_i} \tag{6.34}$$

Suppose the operating frequency is away from cutoff frequency, it can be assumed that only interaction with forward propagating wave in *z* direction, so

$$q_l(z,t) = d_l\, \mathrm{e}^{\left[a_l(t) - \mathrm{i} b_l(t) - \mathrm{i} k_{z_l}\right] z} \tag{6.35}$$

$$\frac{\partial q_l}{\partial t} = d_l \left[a_l'(t) - \mathrm{i}\, b_l'(t)\right] z.\mathrm{e}^{\left[a_l(t) - \mathrm{i} b_l(t) - \mathrm{i} k_{z_l}\right] z} \tag{6.36}$$

$$\frac{d^2 q_l}{dz^2} = d_l \left[a_l(t) - \mathrm{i}\left(b_l(t) + k_{z_l}\right)\right]^2 \mathrm{e}^{\left[a_l(t) - \mathrm{i} b_l(t) - \mathrm{i} k_{z_l}\right] z} \tag{6.37}$$

where $a_l(t)$, $b_l(t)$ are unknown real functions of time, $d_l = q_l(0,t)$ is the input value of q_l, which can be determined by the input power [Wang *et al.* (2014)]. Substituting equation (6.36)-(6.37) in (6.34), separate real and imaginary parts of the equation, then after some simplification for multimode we can obtain

$$\frac{da_l}{dt} = -\frac{c^2}{\omega l_w}\left[2a_l b_l + 2a_l k_{z_l} + \mathrm{Im}\left(\overline{S_l}\right)\right] \tag{6.38}$$

$$\frac{db_l}{dt} = \frac{c^2}{\omega l_w}\left[a_l^2 - b_l^2 - 2b_l k_{z_l} - \mathrm{Re}\left(\overline{S_l}\right)\right] \tag{6.39}$$

where

$$\overline{S_l} = \frac{1}{l_w}\int_0^{l_w}\left(\frac{S_l}{q_l}\right)dz \tag{6.40}$$

where l_w is the length of the waveguide interaction region. Equation (6.38)-(6.39) is the time domain ordinary differential equations that give instantaneous amplitude of the field.

6.2.1. The Dynamic Equations of the Electrons

The electron position coordinates r and θ are rapidly oscillating functions of z. For convenience and clarity, we may define the position coordinates r_c and ψ of the instantaneous guiding centre $(\rho,\varphi,\mathrm{z})$ in terms of r,θ, and perpendicular momentum p_t of the electron by the following equations in the triangle OAB of Figure 6.1,

$$r\sin\left(\frac{\pi}{2}-\phi+\theta\right) = r_b\sin\left(\frac{\pi}{2}+\phi-\psi\right) \tag{6.41}$$

$$r\cos\left(\frac{\pi}{2}-\phi+\theta\right) + r_b\cos\left(\frac{\pi}{2}+\phi-\psi\right) = r_L \tag{6.42}$$

For the equation of motion, we get

$$r_b e^{i\psi} = re^{i\theta} + ir_L e^{i\phi} \tag{6.43}$$

Replacing r_L with $p_t / m_{e0}\Omega$ and differentiating the above equation with respect to z

$$\frac{d}{dz}\left(r_b e^{i\psi}\right) = \frac{d}{dz}\left(re^{i\theta}\right) + i\frac{d}{dz}\left(\frac{p_t}{m_0\Omega}e^{i\phi}\right) \tag{6.44}$$

The first term on the right hand side of the above equation can be written as

$$\frac{d}{dz}\left(re^{i\theta}\right) = \frac{1}{v_z}\frac{d}{dx}\left(x+iy\right) = \frac{\gamma m_0}{p_z}(v_x + iv_y) = \frac{p_t}{p_z}e^{i\phi} \tag{6.45}$$

Substituting the value from equation (6.45) in equation (6.44) and equating the real and imaginary parts, we obtain

$$\frac{dr_b'}{dz'} = \frac{1}{m_e\Omega}\left[p_t\left(\frac{m_e\Omega}{p_z} - \frac{d\phi}{dz}\right)\cos\left(\phi-\psi\right) - \left(\frac{dp_t}{dz} - p_t\frac{\Omega'}{\Omega}\right)\sin\left(\phi-\psi\right)\right] \tag{6.46}$$

$$\frac{d\psi}{dz'} = \frac{1}{r_b m_e k\Omega}\left[\left(\frac{dp_t}{dz} - p_t\frac{\Omega'}{\Omega}\right)\cos(\phi-\psi) + p_t\left(\frac{m_e\Omega}{p_z} - \frac{d\phi}{dz}\right)\sin(\phi-\psi)\right] \tag{6.47}$$

Rearranging the above equation and using the equation $(3.65)-(3.67)$, we can write equation (6.46) and (3.271) as

$$\frac{dr_b'}{dz'} = \left(\frac{p_t}{p_z} + \frac{\omega}{\Omega\beta_z}\left(F_r' + R_r'\right)\right)\cos\left(\phi-\psi\right) - \frac{\omega}{\Omega\beta_z}\left(F_\varphi' + R_\varphi'\right)\sin\left(\phi-\psi\right) \tag{6.48}$$

$$\frac{d\psi}{dz'} = \left[\frac{\omega}{r_b k\Omega\beta_z}\left(F_\varphi' + R_\varphi'\right)\cos\left(\phi-\psi\right) + \frac{p_t}{r_b k}\left(\frac{1}{p_z} + \frac{\omega}{\Omega p_t\beta_z}\right)\left(F_\rho' + R_r'\right)\right]\sin\left(\phi-\psi\right) \tag{6.49}$$

Now, calculating the Lorentz force component by using the equation (3.48)

$$F_r' = -\frac{e}{\omega m_{e0}c}(E_r + v_t B_z - v_z B_\varphi) \tag{6.50}$$

$$F_\varphi' = -\frac{e}{\omega m_{e0}c}(E_\varphi + v_z B_\rho) \tag{6.51}$$

$$F_z' = \frac{e}{\omega m_{e0} c} v_z B_\rho \tag{6.52}$$

$$R_r' = 0 \tag{6.53}$$

$$R_\varphi' = \frac{g_t \beta_t \beta_z}{k} \tag{6.54}$$

$$R_z' = -\frac{g_t \beta_t^2}{k} \tag{6.55}$$

Substituting the electric and magnetic field component from equation $(6.22)-(6.27)$ into Lorentz force component, we obtain force component in term of electric and magnetic fields,

$$F_r' = -\frac{e\mu_0}{\omega m_{e0} c} \mathrm{Re} \sum_{l=1}^{L} \left\{ \sum_{s=-\infty}^{s=\infty} -\frac{s\omega}{r_L k_{t_l}^2} p_l(z,t) + v_t q_l + v_z \frac{is}{r_L k_{t_l}^2} q_l' \right\} J_s(k_{t_l} r_L) J_{m-s}(k_{t_l} r_b) \mathrm{e}^{i(\omega t - (m_l - s)\psi - is\varphi)} \tag{6.56}$$

$$F_\varphi' = -\frac{e\mu_0}{\omega m_e c} \mathrm{Re} \sum_{l=1}^{L} \left\{ \sum_{s=-\infty}^{s=\infty} \frac{i\omega}{k_{t_l}} p_l + \frac{v_z}{k_{t_l}} q_l' \right\} J_s'(k_{t_l} r_L) J_{m-s}(k_{t_l} r_b) \mathrm{e}^{i(\omega t - (m_l - s)\psi - is\varphi)} \tag{6.57}$$

$$F_z' = \frac{e\mu_0 v_t}{\omega m_e c k_{t_l}} \mathrm{Re} \sum_{l=1}^{L} \left\{ \sum_{s=-\infty}^{s=\infty} q_l' J_s'\left(k_{t_l} r_b\right) \right\} J_s(k_{t_l} r_L) J_{m-s}(k_{t_l} r_b) \mathrm{e}^{i(\omega t - (m_l - s)\psi - is\varphi)} \tag{6.58}$$

Put the value of force component in $(3.65)-(3.67)$, we can obtain

$$\frac{dp_z'}{dz'} = -\frac{g_t \beta_t^2}{k \beta_z} + \frac{e\mu_0 \beta_t}{\omega m_e \beta_z} \mathrm{Re} \sum_{L=1}^{N} \left\{ \sum_{s=-\infty}^{s=\infty} \frac{1}{k_{t_l}} \frac{\partial g}{\partial z} J_s'\left(k_{t_l} r_L\right) J_{m_l - s}\left(k_{t_l} r_b\right) \mathrm{e}^{i(\omega t - (m_l - s)\psi - is\varphi)} \right\} \tag{6.59}$$

$$\frac{dp_t'}{dz'} = \frac{g_t}{k} \beta_t - \frac{e\mu_0}{\omega m_e \beta_z} \mathrm{Re} \sum_{l=1}^{L} \left\{ \sum_{s=-\infty}^{s=\infty} \frac{1}{k_{t_l}} \left(\frac{i\omega f_l}{c} + \beta_z q_l' \right) J_s'\left(k_{t_l} r_L\right) J_{m-s}\left(k_{r_l} r_b\right) \mathrm{e}^{i(\omega t - (m_l - s)\psi - is\varphi)} \right\} \tag{6.60}$$

$$p_t'\left(\frac{d\phi}{dz}-\frac{\mu}{p_z'}\right)=-\frac{e\mu_0}{\omega m_e\beta_z}\mathrm{Re}\sum_{l=1}^{L}\left\{\sum_{s=-\infty}^{\infty}\left(-\frac{\omega s p_l}{r_L c}-k_{t_l}^2\beta_t q_l-\frac{is}{r_L}\beta_z q_l'\right)\right.$$
$$\left.J_s\left(k_{t_l}r_L\right)J_{m_l-s}\left(k_{t_l}r_b\right)\mathrm{e}^{i(\omega t-(m_l-s)\psi-is\varphi)}\right\} \tag{6.61}$$

$$r_b'\frac{d\psi}{dz'}=\frac{e\mu_0}{\omega m_{e0}\mu\beta_z}\left\{\sum_{l=1}^{L}\sum_{s=-\infty}^{\infty}\frac{(m-s)}{k_{m_l n_l}^2 r_b}J_s(k_{t_l}r_L)J_{m-s}(k_{t_l}r_b)\,\mathrm{Im}\left\{\left(\frac{i\omega p_l}{c}+\beta_z q_l'\right)\mathrm{e}^{i(\omega t-(m_l-s)\psi-is\varphi)}\right\}-\right.$$
$$\left.\sum_{l=1}^{L}\sum_{s=-\infty}^{\infty}\left(J_{s-1}\left(k_{t_l}r_L\right)J_{m-s+1}(k_{t_l}r_b)\right)+J_{s-1}\left(k_{t_l}r_L\right)J_{m-s-1}(k_{t_l}r_b)\,\mathrm{Re}\left\{\frac{1}{2}\beta_t q_l\,\mathrm{e}^{i(\omega t-(m_l-s)\psi-is\varphi)}\right\}\right\} \tag{6.62}$$

$$\frac{dr_b'}{dz'}=-g_t r_b+\frac{e\mu_0}{\omega m_e\mu\beta_z}\sum_{l=1}^{L}\sum_{s=-\infty}^{\infty}\frac{1}{k_{t_l}}J_s(k_{t_l}r_L)J_{m-s}'(k_{t_l}r_b)\,\mathrm{Re}\left(\frac{i\omega p_l}{c}+\beta_z q_l'\right)\mathrm{e}^{i(\omega t-(m_l-s)\psi-is\varphi)}$$
$$+\frac{e\mu_0}{\omega m_e\mu\beta_z}\sum_{L=1}^{N}\sum_{s=-\infty}^{\infty}\left(J_{s+1}\left(k_{t_l}r_L\right)J_{m-s-1}(k_{t_l}r_b)\right)-J_{s-1}\left(k_{t_l}r_L\right)J_{m-s+1}(k_{t_l}r_b)$$
$$.\mathrm{Im}\left\{\frac{1}{2}\beta_t q_l\,\mathrm{e}^{i(\omega t-(m_l-s)\psi-is\varphi)}\right\} \tag{6.63}$$

and

$$\frac{dt}{dz}=\frac{\gamma m_e}{p_z} \tag{6.64}$$

For initial phase of the electron, it assumed that they are uniformly distributed over the interval $(0,2\pi)$. For the initial distribution in space, it is assumed the electron beam is annular with all the guiding centres uniformly distributed on the circle of the radius r_b and around each guiding centre is a ring of electrons uniformly spaced in their common Larmor orbit. Equation $(6.59)-(6.64)$ has completely described the evolution of electrons in the interaction region of the gyro-TWT amplifier.

Power and Efficiency

The power propagating along the interaction circuit is calculated using the Poynting's vector and can be given by

$$P = \frac{c}{8\pi}\int_0^{r_w} r dr \int_0^{2\pi} \mathrm{Re}\left[\vec{E}\times\vec{B}^*.\hat{z}\right] \tag{6.65}$$

The corresponding electronic efficiency of gyro-TWT amplifier is defined as the ratio of the grown RF power to the applied DC beam power and is estimated as

$$\eta = \frac{\beta_{to}^2}{2(1-1/\gamma)(1-h\beta_{z0})}\eta_t \tag{6.66}$$

where, $\eta_\perp$ is the orbital efficiency which characterizes the changes in the electron orbital momentum in the interaction mechanism.

6.2.2. *Algorithm for multimode LSA of Gyro-TWT Amplifier*

- **Step 1**: Start t=0, d=d_0 consider $g(z,t) = d\,\mathrm{e}^{\{-\mathrm{a}(t)+\mathrm{ib}(t)\}+\mathrm{i}k_z z}$ calculate $g(z,t)\big|_{z=0 to L}$ complete g at $t=0$ along the waveguide $g = \left[g_{z=0}\ \ g_{z=1}\ \ldots\ldots\ldots\ldots\ g_{z=L}\right]$.
- **Step 2**: Calculate $\mathcal{F}$ using A', which is $A = g$, we have $F = \left[F_{z0}\ \ F_{z1}\ldots\ldots\ldots\ldots\ldots \mathrm{F}_{zL}\right]$.
- **Step 3**: With the help of $F = \left[0\ \ 1\ldots\ldots\ldots\ldots\ldots \mathrm{L}\right]$, calculate $\{w\,\&\,v_s\}$ along the waveguide with the help of coupled equation i.e. $\frac{dw}{dz}, \frac{dv_s}{dz}$.
- **Step 4**: Since, we need to move from $t = t_0$ to t_1 , so we need updated ($a\,\&\,b$). For that $\frac{da}{dt} = f(\mathrm{a},\mathrm{b},\mathrm{S})$ and $\frac{da}{dt} = f(\mathrm{a},\mathrm{b},\mathrm{S})$ to solve where S is $f(\mathrm{w},v_s)$, find new S value.
- **Step 5**: Consider past a,b and updated S values to get new updated a and b.
- **Step 6:** Updated a,b gives new g values at $t = t_1$, repeat from step 2.

6.2.3. *Flow-chart for multimode LSA of Gyro-TWT Amplifier*

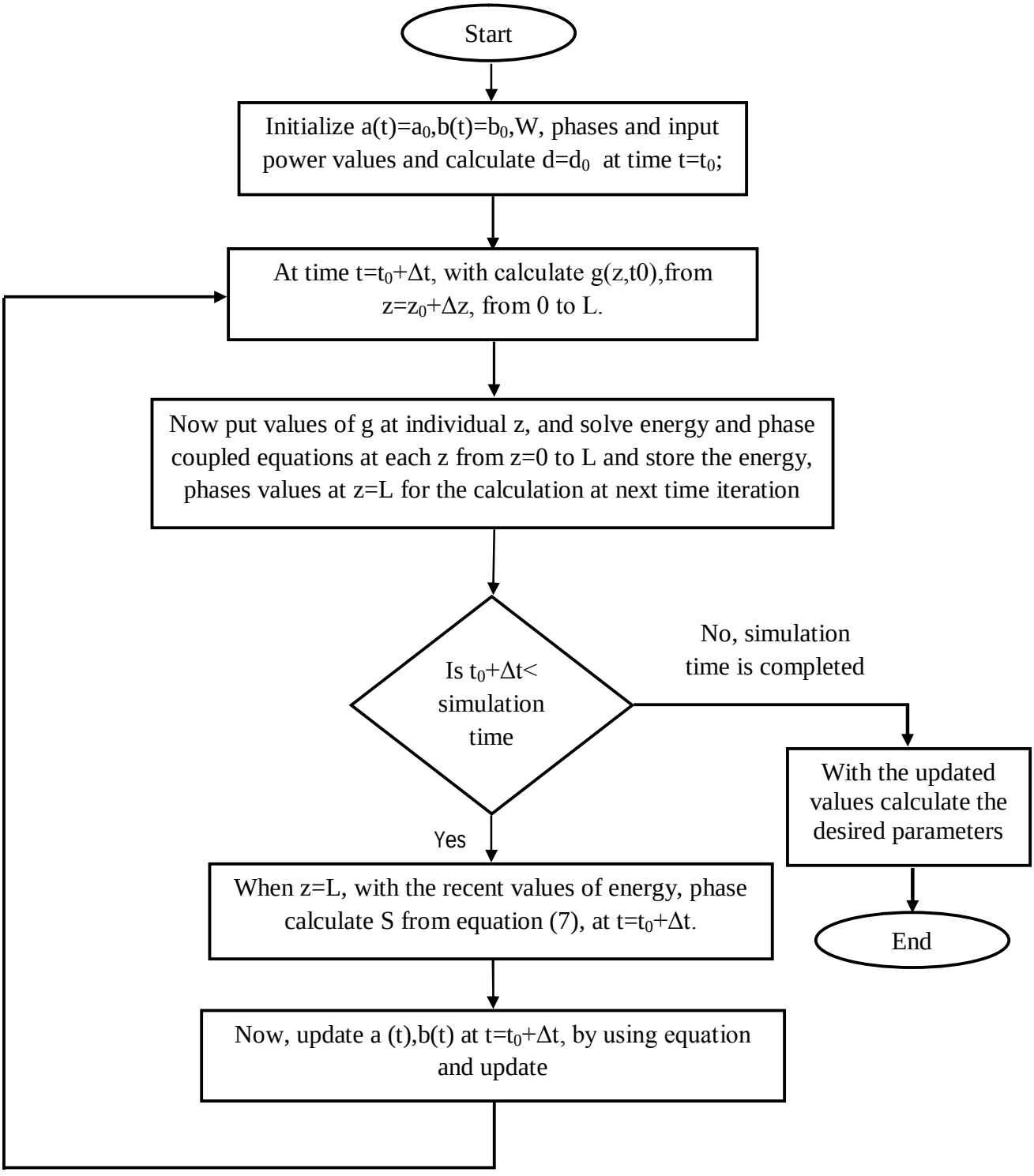

Figure 6.2. Flow chart for the performance estimation of multimode gyro-TWT amplifier.

6.3. Results and Discussion

The generalized single particle time dependent and time independent multi-mode nonlinear analyses developed in the preceding section 6.2 are further exploited to observe the gyro-TWT amplifiers behaviour with the aid of numerical computations. To validate the developed analytical model, *W*-band gyro-TWT amplifier described and taken in the earlier Chapters of this thesis is selected again. This performance estimation has been carried for the validation of the developed analysis, so that they can be successfully implemented for the design and analysis of the higher harmonic mode operated gyro-TWT amplifiers.

The analysis of 91.4GHz, second harmonic gyro-TWT with operating in the TE_{02} mode has been carried out using the approach developed above. Table 5.1 shows the design specifications taken for analysis of 91.4GHz gyro-TWT.

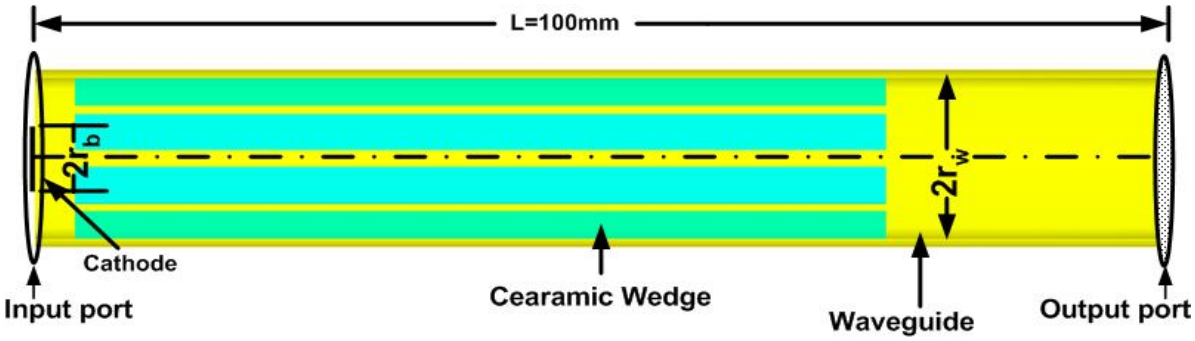

Figure 6.3. Cross sectional view of ceramic loaded gyro-TWT.

A computer code has been developed in the MATLAB based on the multimode nonlinear analysis described in the previous section to investigate the RF behaviour of the gyro-TWT as well as validate the developed analysis. In the time dependent multimode analysis, the differential equations are solved using Runge-Kutta method. For the 128 number of particles, accuracy is found to be sufficient enough. All the electrons are

assigned the initial transverse and longitudinal energy based calculated from the beam voltage (V_b) and the velocity pitch factor (α). The electrons are uniformly distributed over the interval [0, 2π] for the zero velocity spread. For the multimode analysis, a computer code has also written to analyse the interaction mechanism. This code provides the comprehensive picture of the multimode effect on the performance of the device for arbitrary harmonic operation. The coupling coefficient between the electron beam and RF fields in the cylindrical waveguides is defined as

$$C_{mn} = \frac{J_{m\pm s}^2(k_t r_b)}{(v_{mn}^2 - m^2)J_m^2(v_{mn})} \qquad (6.67)$$

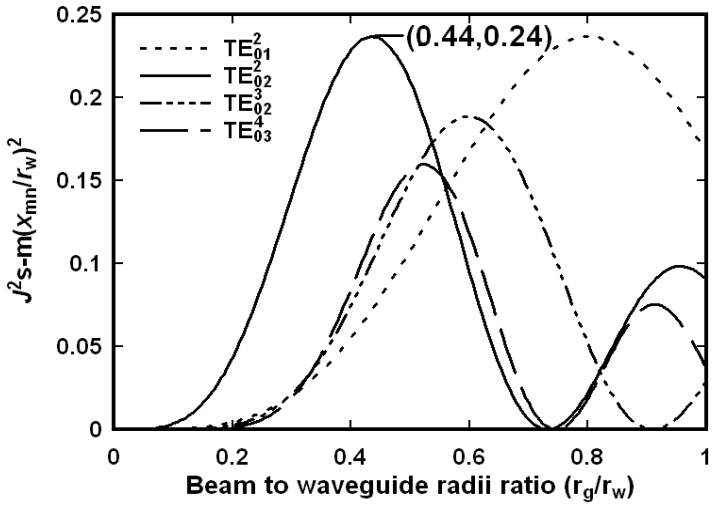

Figure 6.4. Coupling coefficient C_{mn} as a function of ratio of beam to waveguide radii (r_b/r_w) for the different modes.

Using this expression, the optimum radius of the electron beam can be determined for the maximum coupling to the chosen mode. The normalized coupling coefficient (C_{mn}) of second-harmonic TE_{02} mode gyro-TWT amplifier and competing modes with respect to the normalized beam radius for the different number of modes is shown in Fig. 6.4.

The peak value of coupling coefficient for the desired mode at $r_g / r_w = 0.44$. However to reduce the interaction strength of nearby competing, a value for r_g / r_w of 0.41 is selected. The temporal growth of the RF output power for the operating TE_{02}^2 mode and the other nearby competing modes (TE_{01}^2 and TE_{02}^3) has been shown in Figs. 6.5.

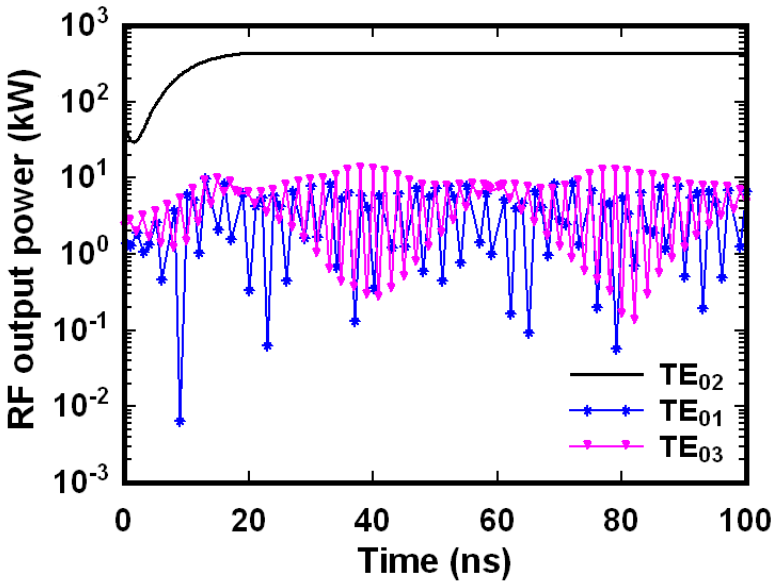

Figure 6.5. Temporal growth of the RF output power in the operating TE_{02}^2 and competing mode (TE_{01}^2 and TE_{02}^3).

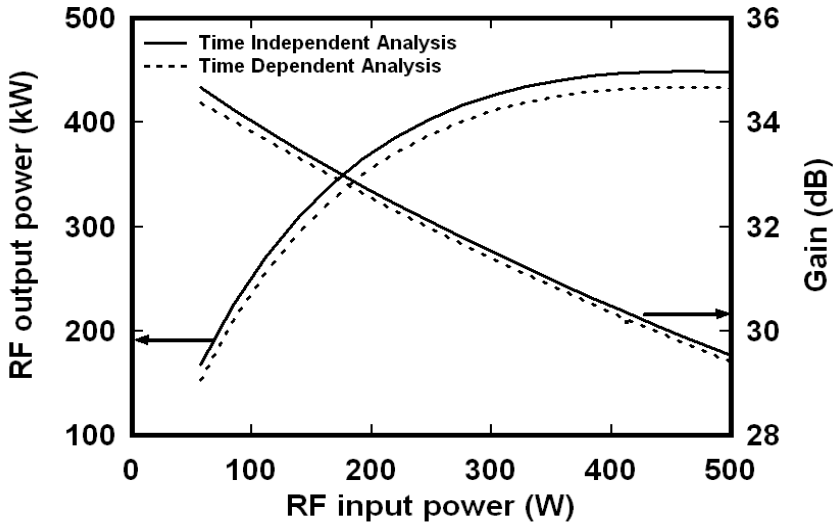

Figure 6.6. Comparison in variation of RF output power and gain with drive power.

Figs. 6.5 explicitly demonstrate that none of the competing mode has sufficient power apart from desired mode. It indicates that a stable RF output power of ~438kW. Fig. 6.6 elucidates the variation of RF output power and gain with the drive input power. By time independent single mode analysis and time dependent multimode analysis has RF saturated power ~450kW and ~438kW, respectively, and corresponding saturation gain are ~30dB and ~29.88dB, respectively. Figure 6.7 shows the comparison in variation of RF output power and gain with pitch factor. By time independent analysis the peak power and gain is ~450kW and ~30dB, respectively and through time dependent analysis the peak power and gain is ~435kW and ~29.88dB, respectively.

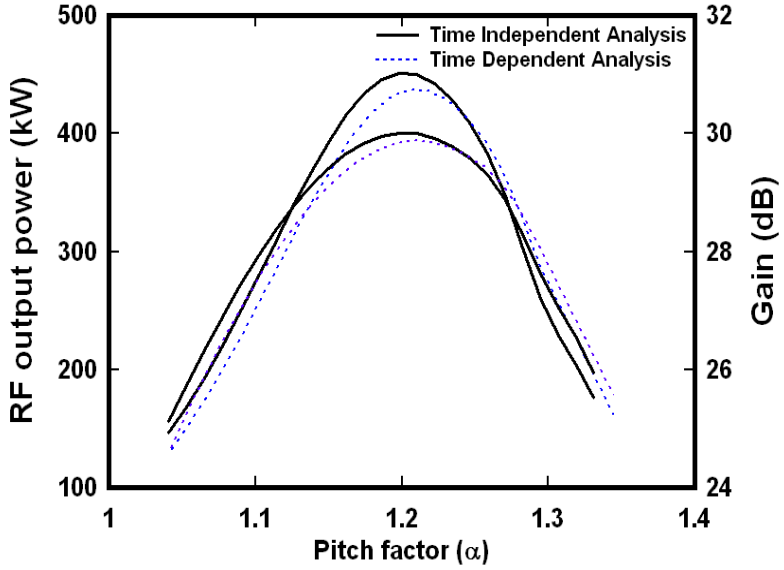

Figure 6.7. Comparison in variation of RF output power and gain with pitch factor.

Fig. 6.8 depicts the variations of RF output power with the drive frequency. The variation of RF power through CST PIC simulation software, time dependent analysis and time independent analysis, results are closely matched, at saturation its peak value is ~435.6kW, ~438kW and ~450kW, respectively.

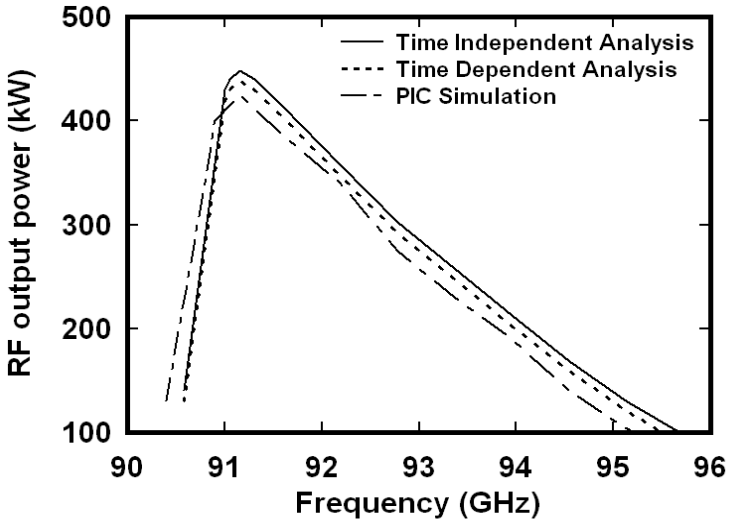

Figure 6.8. Comparison in variation of RF output power with frequency.

6.4. Conclusion

For the gyro-TWT operating at the higher harmonic, for the reduction of the magnetic field requirements, we use overmoded RF structure. Hence, there is necessity to study the other competiting modes along with the fundamentals. For the analysis of a gyro-TWT amplifier, both time independent and time dependent signal analyses are in vogue. Small signal analysis based on the linear theory is used to study the device behaviour in the linear regime. On the other hand, the large signal analysis based on the nonlinear theory is used to predict output power, efficiency, saturated gain, and phenomenon of electron cross-over and bunching thereby providing better understanding of the beam-wave interaction and saturation mechanisms. A self-consistent time-dependent multi-mode nonlinear signal formulation for the gyro-TWT has been developed in the present Chapter to study the beam-wave interaction behaviour of a gyro-TWT amplifier considering all the competiting modes into the consideration. The addition of waveguide wall loss is a solution to suppress the competing modes in the gyro-TWT has also been studies. In loading technique, lossy

ceramic attenuating material is deposited on the waveguide wall. Through the introduction of additional losses, convective instability amplification is reduced and hence increases the start oscillating current of nearby competing modes. The coupling coefficient provides the selection of beam guiding centre radius for a particular mode of operation. In order to get optimum beam-wave interaction, it is important to position the electron beam at the place where field is the maximum. The output power and efficiency depend on the beam interaction quality. The selection of appropriate value of axial magnetic field is important for proper beam-wave interaction in order to get optimum saturated power.

The effects of the various device parameters, such as, variations in the pitch factor, drive power, and drive frequency on the bandwidth and RF output power has also been explored and discussed. This sensitivity studies will help this device developer to analyse their device under practical conditions. The analytical results obtained by the large signal analysis developed in the present chapter have also been validated with the PIC simulation values obtained using available 3D commercial software CST in the previous chapter.

In the next chapter, summary and conclusion is discussed. Further limitations of the present work and scope for and future work is also discussed.